Electrical Transport Properties of the Si(111) Surface with Control of Its Atomic-Scale Structure

S. Hasegawa, Z.H. Zhang, C.S. Jiang, and S. Ino*

Department of Physics, Faculty of Science, University of Tokyo,
Hongo, Bunkyo-ku, Tokyo 113, Japan
*also at PRESTO, Research Development Corporation of Japan,
1-1-4 Umezono Tsukuba-shi, Ibaraki 305, Japan

Abstract. We discuss the atomic-scale structure control and the resulting electric properties of Si(111) surfaces with some surface superlattice structures. *In-situ* measurements of surface conductance, Hall effect, and field effect clearly revealed the difference between the Si(111)-7 × 7 clean surface and the Si(111)-$\sqrt{3} \times \sqrt{3}$-Ag surface. The atomic arrangements and the characteristic surface electronic states govern the Fermi-level pinning and band bending which determine the electrical properties of the surfaces.

1. Introduction

The atomic-scale analysis and control of structures of solid surfaces have now been within our scope in the light of a variety of sophisticated surface science techniques, especially scanning tunneling microscopy (STM). Recent STM techniques allow one not only to image the atomic arrangements of surfaces, but also to "manipulate" individual atoms adsorbed on a surface, which opens up a possibility of constructing ultimate nanoscale structures on a surface, far beyond the present micro-fabrication technology [1]. The resulting surface electronic states are also probed at the atomic resolution by scanning tunneling spectroscopy (STS) techniques [2]. These demonstrations have stimulated the researchers in a wide range of fields of science and technology to expect possible applications to studies on novel solid state physics as well as device fabrications.

Another approach to control the atomic structures of surfaces, which seems more practical at the present stage, is precise control of various kinds of phenomena occurring on the surface, e.g, epitaxy, reconstruction, migration, and desorption. One of the most well known applications of epitaxy techniques is superlattice structures of GaAs/GaAlAs, having coherency in stacking of atomic layers normal to the surface and atomically abrupt hetero-interfaces. Several techniques such as migration-enhanced epitaxy (MEE) [3] and surfactant epitaxy [4] have been proposed for improving the quality of the grown thin crystal. These techniques enable precise controls of atomic-layer stacking vertically coherent with the substrate lattice.

A method is also proposed to construct a "lateral superlattice" using regularly arranged atomic steps on a vicinal surface [5]. Step-flow growth is successfully employed to stack the deposited atoms at the step edges on a surface in a later-

Springer Series in Materials Sciences, Vol. 31 **Nanostructures and Quantum Effects**
Editors: H. Sakaki · H. Noge

ally ordered manner. The first material such as GaAs is deposited to cover the back portion of each terrace, and then enough amount of the second material such as AlAs is deposited to cover the remaining front portion of the terraces. The step edges then return to their original locations. This process results in a coherent lateral structures having a lateral period of the terrace width.

Lateral coherency in geometric structures on surfaces can be modulated also by "surface reconstruction". Surface superlattice structures, which have a periodicity different from the simple truncated face of a bulk crystal, appear on clean surfaces (such as Si(111)-7 × 7) as well as on foreign-atom adsorbed surfaces (such as Si(111)-$\sqrt{3} \times \sqrt{3}$-Ag). In some cases, several different surface superlattice structures appear on the same crystal surface depending on the conditions, and their nature drastically changes. Utilizing these facts, some kinds of nanoscale structures may be fabricated to bring out some functional properties. The artificially constructed atomic arrangements laterally or normally near surface region in this way (superlattices and coherent ultra-thin films, or in some cases, three-dimensional superlattice structures) raise various kinds of interesting properties that provide rich field of study.

Recent experiments on Schottky barriers with well-controlled interface structures of some metal-semiconductor pairs have demonstrated the dominant role of the local interface structures over macroscopic bulk parameters playing in determination of the barrier height [6-8]. Electrical conductance of silicon surface also has been found to change crucially depending on the surface superlattice structures [9]. Changes in atomic arrangements in only one or two atomic layers at surfaces/interfaces actually influence the macroscopic electric properties.

In this paper we discuss the atomic structure control and the resulting electric properties of Si(111) surfaces with some superlattice structures. Structure-dependent surface conductance, Hall effect, and field effect, simultaneouly measured with RHEED (reflection-high-energy electron diffraction) observations in ultrahigh vacuum are reported.

2. Si(111)-7 ×7 and Si(111)-$\sqrt{3} \times \sqrt{3}$-Ag Surfaces

Figure 1(a) shows a RHEED pattern from a clean Si(111)-7 × 7 surface, and (b) is the atomic arrangement of the well-known DAS (dimer-adatom-stacking fault) model for this surface [10]. The lozenge of the 7 × 7-unit cell contains two triangles separated by the dimer chains. Each triangle has six adatoms (the biggest filled circles) and three "rest atoms"(the medium-sized filled circles). Valence-band photoemission spectroscopy shows three conspicuous surface states S_1, S_2, and S_3 around 0.2, 0.9, and 1.8 eV, respectively, below the Fermi level, as schematically shown in Fig. 1(c) [11,12]. S_1 peak is assigned to the dangling bond state on the 12 adatoms. Since this state extends to the Fermi level, it is considered to be half-occupied, i. e., a metallic state. The Fermi level is pinned at this state due to its high density of states. Its position E_F with

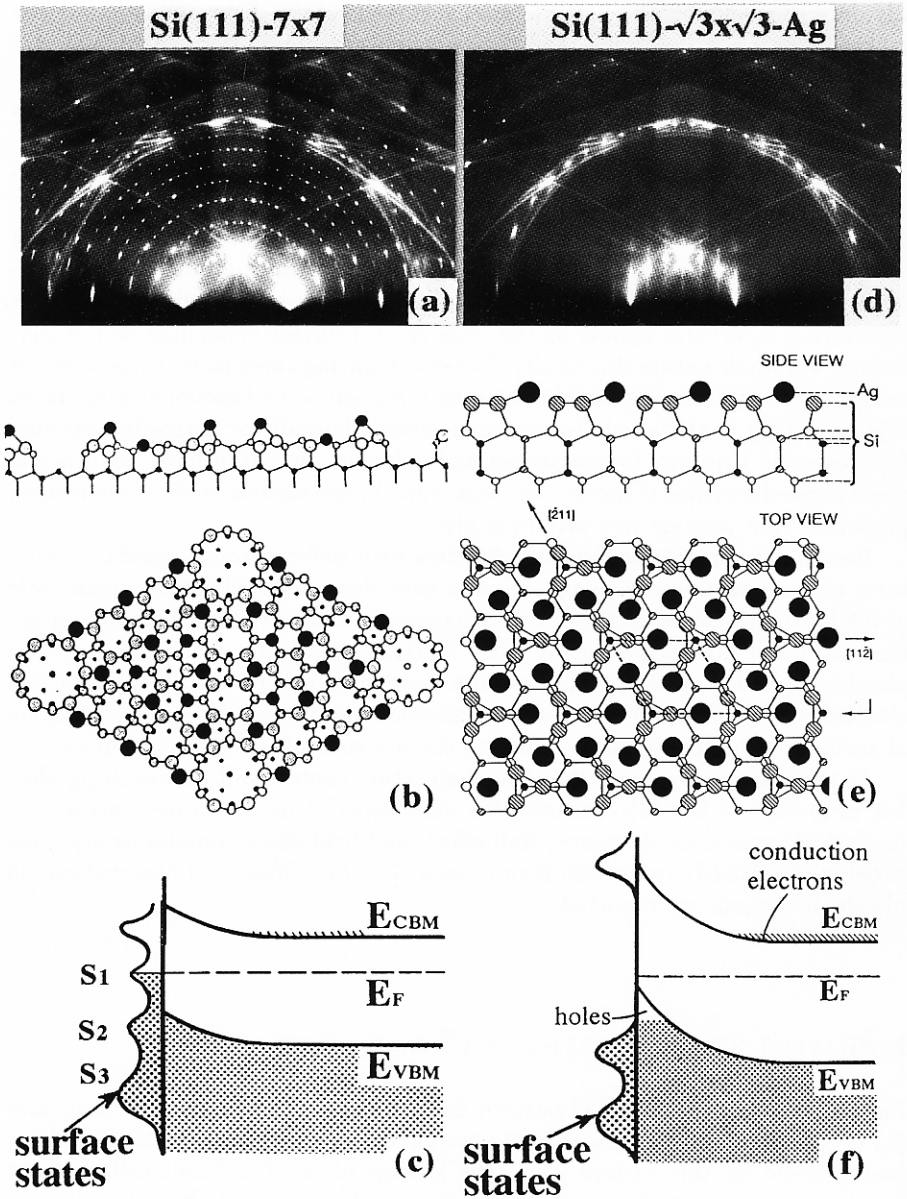

Fig. 1. Si(111)-7 × 7 clean surface and Si(111)-$\sqrt{3} \times \sqrt{3}$-Ag surface. (a)(d) RHEED patterns, (b)(e) schematic illustrations of atomic arrangements, and (c)(f) schematic energy-band diagrams under the surfaces for an n-type Si wafer, respectively.

respect to the valence band maximum E_{VBM} at this surface is measured to be $E_F - E_{VBM} = 0.63$ eV [13]. Since this position is around the middle of the band gap, the surface space-charge layer beneath the 7×7 structure always exhibits a depletion layer, irrespective of doping type of the bulk Si.

When Ag of 1ML (monolayer) is deposited on the Si(111)-7×7 substrate maintained above $250°C$, the surface structure is converted into a $\sqrt{3} \times \sqrt{3}(R30°)$ periodicity (Fig. 1 (d)). For this surface, a honeycomb-chained trimer (HCT) model (Fig. 1(e)) [14] is found to be consistent with most of reported experimental results and first-principles calculations. The $\sqrt{3} \times \sqrt{3}$-unit contains three Ag atoms. So the number of valence electrons in the unit cell is even, three from Ag atoms and nine from dangling bonds of three Si atoms. This is consistent with the semiconducting character of this surface, contrasting to the metallic nature of the Si(111)-7×7 surface. Photoemission and inverse photoemission spectroscopies show a distinct energy gap around the Fermi level. Core-level shifts in soft X-ray photoemission spectroscopy [15] show an E_F position very close to the E_{VBM} (0.13~0.15 eV above the E_{VBM}) at this surface. So the bands are found to bend upward enough to create a p-type inversion layer on an n-type Si bulk (Fig. 1(f)) or an accumulation layer on a p-type substrate.

3. Surface Conductance

We prepared a Si(111) wafer of $5 \times 20 \times 0.4mm^3$ in size, a half of which surface was covered with the $\sqrt{3} \times \sqrt{3}$-Ag superlattice and another half remained in the clean 7×7 structure, by masking the half of the surface from the Ag evaporator (Fig. 2(a)). The resistance of each surface area was simultaneously measured with two pairs of voltage pick-up Ta-wire contacts with small constant current flowing at room temperature (RT). Since the resistance sensitively depended on the heat treatments for cleaning and preparing the surface superlattices, the two surface areas having the same heat-treatment history had to be prepared on a single silicon wafer. The difference in resistance measured in this way is attributed only to the difference in surface conductance with different surface superlattice structures. The result was that the $\sqrt{3} \times \sqrt{3}$-Ag area is more conductive than the 7×7 area by 1.15×10^{-4}A/V with a p-type Si wafer of $20\ \Omega \cdot cm$ resistivity. This difference is quantitatively explained by the difference in conduction through the surface space-charge regions between the two surfaces, an accumulation layer for the $\sqrt{3} \times \sqrt{3}$-Ag surface and a depletion layer for the 7×7 surface [16]. Although silver of the amount of 1ML does adsorb in the $\sqrt{3} \times \sqrt{3}$-Ag phase, conduction through this Ag layer does not set on. This is because the Ag atoms make covalent bonds with the substrate Si atoms, and do not have delocalized electrons for metallic conduction. Since, on the other hand, the 7×7 surface has a metallic surface-state band, the conduction via this band may be expected. But its contribution is negligibly small compared with the conduction through the space-charge layer [17]. The surface conductance in

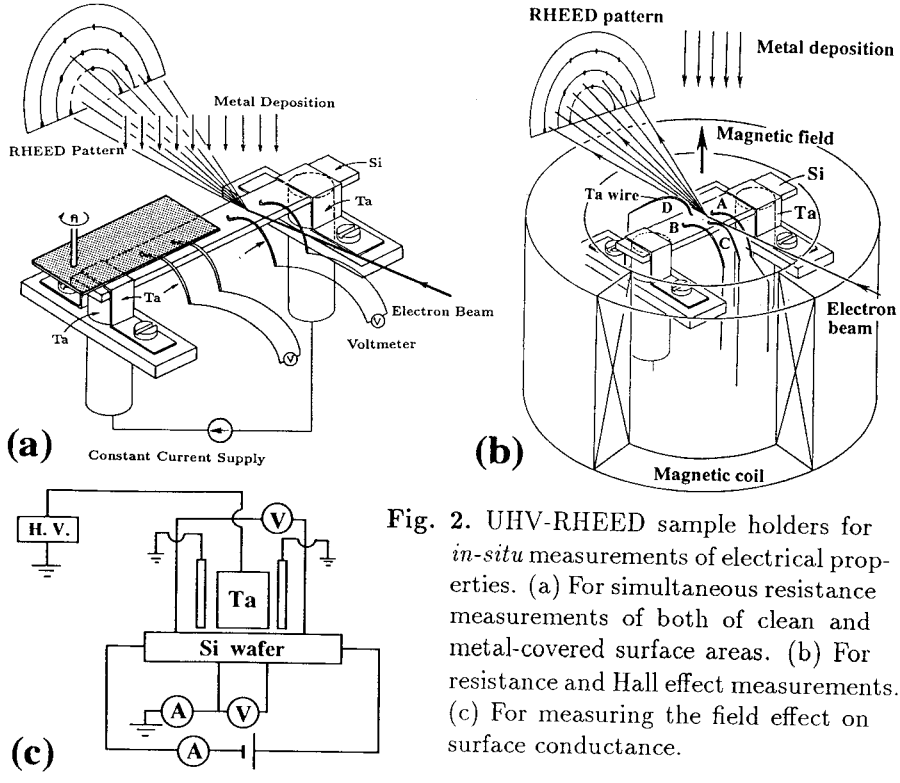

Fig. 2. UHV-RHEED sample holders for *in-situ* measurements of electrical properties. (a) For simultaneous resistance measurements of both of clean and metal-covered surface areas. (b) For resistance and Hall effect measurements. (c) For measuring the field effect on surface conductance.

our experiment is then explained mainly by the band bending at the sub-surface region. The metallic surface-state conductivity of the 7×7 structure is detected as a leak current of a nanoscale metal/Si Schottky contact made of STM tip [18].

4. Atom Dynamics and Surface Conductance

When further Ag was deposited onto the $\sqrt{3}\times\sqrt{3}$-Ag at RT, then, a transmission-type ring pattern from Ag micro-crystals, with spots in some preferential orientations, gradually emerged in the RHEED pattern, while the $\sqrt{3} \times \sqrt{3}$ spots remained unchanged [9]. This means that the deposited Ag atoms nucleate into 3D islands on the $\sqrt{3} \times \sqrt{3}$ phase and scarcely cover the substrate due to a high surface diffusivity of Ag adatoms.

Ag growth on the 7×7 surface at RT was, on the other hand, quite different. Streaks (a reflection pattern) from Ag thin crystals appeared in the RHEED pattern. This Ag layer is known to grow in quasi-layer-by-layer fashion, consisting of twining two-dimensional (2D) Ag thin crystals in a texture structure.

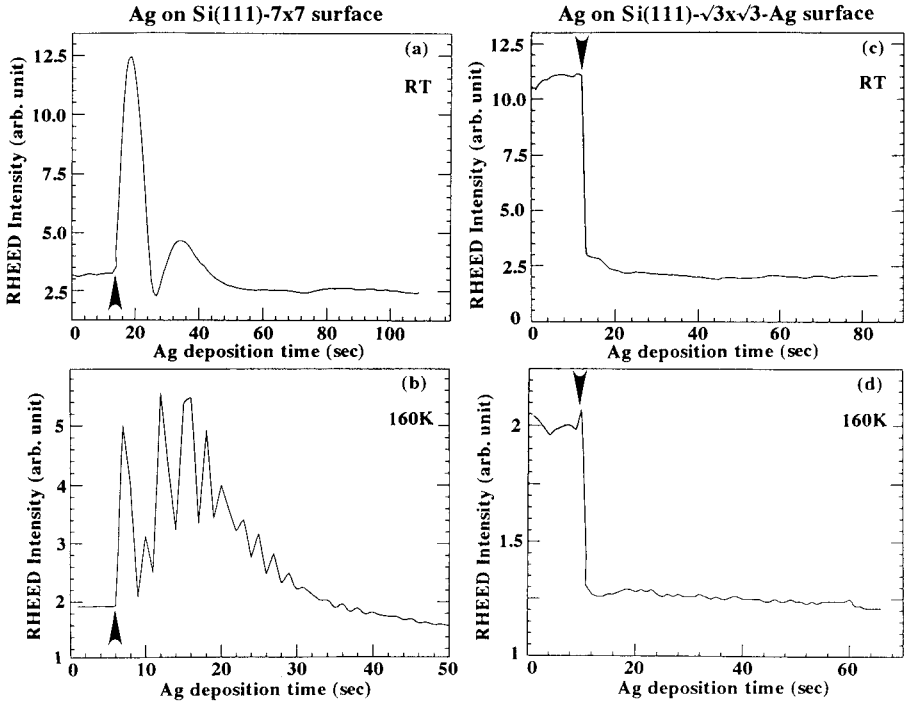

Fig. 3. Changes in intensity of the specular beam of RHEED during Ag depositions onto (a)(b) Si(111)-7 × 7 clean surface or (c)(d) Si(111)-$\sqrt{3} \times \sqrt{3}$-Ag surface, (a)(c) at room temperature or (b)(d) at 160K. The electron beam of 15keV irradiates the surface in $[11\bar{2}]$ incidence with glancing angle of $\sim 0.4°$. Arrow heads indicate the opening of the evaporator shutter.

The dependence of the growth style of Ag layer upon the substrate surface structures are also demonstrated as intensity oscillations of the specular beam of the RHEED (Fig. 3) [19]. During the Ag deposition onto the clean 7 × 7 surface at RT (Fig. 3(a)), two periods of irregular intensity oscillations were observed, while the intensity abruptly dropped and no oscillatory behavior was observed for the $\sqrt{3} \times \sqrt{3}$-Ag surface at RT (Fig.3(c)). Furthermore, as shown in Fig. 3(b), many oscillations with a characteristic change of the background intensity were observed for the 7 × 7 substrate at 160K. This indicates a 2D islands growth (nearly layer-by-layer growth). On the contrary, in the case of the $\sqrt{3} \times \sqrt{3}$-Ag surface at 160K (Fig. 3(d)), the RHEED intensity changed in a similar way as in the case of RT (c). This is a 3D-nuclei growth mode. These results clearly show that an activation energy for surface diffusion of deposited Ag atoms is much smaller on the $\sqrt{3} \times \sqrt{3}$-Ag surface than on the 7 × 7 surface.

What is the correlation between the transport properties and the surface superlattice/epitaxial-growth structures at Ag-covered Si(111) surfaces ? In or-

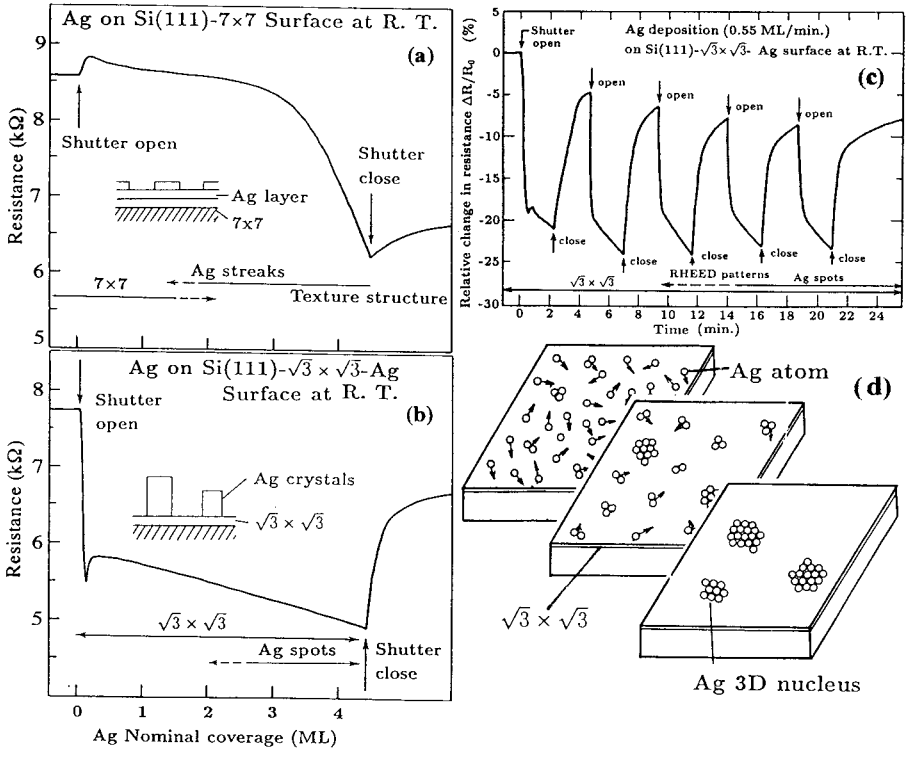

Fig. 4. The changes in resistance of the Si wafer and RHEED patterns during the room-temperature Ag depositions onto (a) the clean Si(111)-7 × 7 and (b) the Si(111)-$\sqrt{3} \times \sqrt{3}$-Ag surfaces. (c) The resistance change during the cycles of room-temperature Ag deposition onto the Si(111)-$\sqrt{3} \times \sqrt{3}$-Ag surface and its interruption. (d) Schematic illustration of nucleation of adsorbed Ag monomers into three-dimensional Ag clusters on the $\sqrt{3} \times \sqrt{3}$-Ag surface.

der to combine the measurements of surface conductance and Hall effect with simultaneous observations of RHEED, a special sample holder shown in Fig. 2(b) was developed [9]. Before each measurement run, the clean 7 × 7 or $\sqrt{3} \times \sqrt{3}$-Ag was prepared by Ag deposition and direct heating by a current fed through the Ta-rod electrodes. The conductance of the central portion of the wafer, under isothermal condition at RT, was measured as a voltage drop between a pair of Ta wire contacts A and B, kept in elastic contact with the wafer, with a constant current of, e.g., 10 μA, supplied through the Ta rod electrodes. The Hall voltage was simultaneously measured through another pair of Ta wire contacts C and D, which were set to be nearly perpendicular to the measuring current. Magnetic field of nearly perpendicular to the wafer surface was applied with a coil. The RHEED beam was always turned off during the measurement, except for the intermittent observations of the RHEED patterns in the course of Ag deposition.

Figure 4(a) shows a change in resistance during Ag deposition (rate: 0.45 ML/min) onto the clean Si(111)-7 × 7 surface of an n-type wafer (50Ω·cm resistivity) at RT [9]. Changes in RHEED patterns in the course of deposition are also shown in the figure. The resistance does not show significant changes until the 7 × 7 pattern disappears around 2∼3 ML coverage, with the exception of a slight increase just after opening the evaporator shutter. The Hall voltage remained almost constant on this initial stage. In response to the subsequent development of a texture structure of the Ag film, the resistance begins to decrease steeply. The Hall voltage also began to drop, meaning a steep increase in carrier concentration. After the deposition off, the resistance slightly raises.

In the case of Ag deposition onto the Si(111)-$\sqrt{3} \times \sqrt{3}$-Ag surface at RT, the resistance changes in a completely different way(Fig. 4(b))[9]. After an abrupt drop in the resistance at the beginning of deposition (less than 0.1 ML deposition), it decreases at a moderate rate during Ag deposition. This change is actually caused by Ag atom adsorption on the substrate, not an influence of radiation from the Ag evaporator [9]. The Hall voltage also abruptly decreased at the beginning of deposition, say from 18 μV to 12 μV, and it remained almost constant after that during Ag deposition. This means an abrupt increase of the carrier concentration at the beginning. The steep raise in resistance after closing the evaporator shutter in Fig. 4(b) corresponds to a process of nucleation of Ag adatoms on the $\sqrt{3} \times \sqrt{3}$-Ag surface as discussed below.

Photoemission spectroscopies reveal microscopic changes in the surface electronic states of the Si(111)-7 × 7 covered with various amounts of Ag at RT [20]. The valence-band spectra show that adsorption of only about 0.2 ML Ag causes a quick suppression of the dangling-bond state at the Fermi level (S_1 state), converting the surface into semiconducting from a metallic 7 × 7. This is consistent with the STS measurements [21]. The Si 2p core-level spectra reveal an overall shift of the entire line shape to lower binding energies, indicating an upward band bending of ∼ 0.26eV by 1ML Ag adsorption. In other words, the Fermi-level is depinned from the metallic S_1 state of the 7 × 7 surface and E_F position shifts from 0.63eV down to 0.37eV above the valence-band maximum E_{VBM}. From a calculation of the surface conductivity $\Delta\sigma$ versus the Fermi-level position [9], the conductivity does not significantly change by this Fermi-level shift (only within a depletion-layer range). This is consistent with the measurement that the resistance shows no remarkable changes in the initial deposition (Fig. 4(a)).

A definite explanation for the observed slight increase in resistance at the very early stage of the deposition in Fig. 4(a) is lacking at present. But, since this change corresponds to the saturation of the dangling-bond state by Ag adsorption, the conversion from a "metallic" surface to a "semiconducting" one may cause such a resistance change. In other words, this may correspond to suppression of electron transport via the metallic surface state of the 7 × 7. The magnitude of this resistance change is not inconsistent with Henzler's estimation of conductivity via a metallic surface-state band [17].

Differential reflectivity spectroscopy reveals that, with further increasing Ag coverage on the 7 × 7 surface, Ag layer becomes metallic from semiconducting

[22]. This is because the initially adsorbed Ag atoms make covalent bondings with the dangling bonds of the Si substrate, resulting in a semiconducting character, while, after the saturation of the dangling bonds, additional Ag atoms undergo metallic bonding between themselves. This process is accompanied by a delocalization of the "$5s$" valence electrons of Ag atoms to be metallic. This must correspond to the steep decrease in resistance at $2\sim$ 3ML Ag coverage in Fig. 4(a). Percolation paths of metallic conduction may be created around this coverage range. 2D Ag islands on the surface more easily create percolation paths than 3D Ag nuclei. So the rates of decrease in resistance in the thicker coverage range (more than 3 ML) are quite different between Figs. 4(a) and 4(b).

Taking into account the fact that the Si(111)-$\sqrt{3} \times \sqrt{3}$-Ag surface is "semiconducting", the Fermi level at the surface is expected to easily shift with the subsequent Ag adsorption. Since the Fermi level is measured to lie at $\sim$0.1eV above the valence-band maximum on the $\sqrt{3} \times \sqrt{3}$-Ag as mentioned in Section 2, the steep drop in resistance at the beginning of the Ag deposition (Fig. 4(b)) must be caused by a further downward shift of the E_F position toward the valence-band maximum (i.e. further upward band bending). This means that Ag atoms deposited on top of the $\sqrt{3} \times \sqrt{3}$-Ag layer act as acceptors, and introduce negatively charged acceptor-like surface states. A very small amount of Ag adatoms is enough to raise such variation. But this change is recovered when the Ag deposition is stopped, leading to a steep increase in resistance. Figure 4(c) shows the resistance change during cycles of Ag deposition and its interruption. Steep decreases and raises in resistance are repeatedly observed at opening and closing the evaporator shutter, respectively. The recovering raise in resistance after the deposition off is considered to correspond to aggregation of the adsorbed Ag atoms on the $\sqrt{3} \times \sqrt{3}$ phase (Fig. 4(d)). This results in decrease of charge transfer between the Ag adatoms and the substrate to prevent the further band bending. In other words, only isolated Ag atoms on top of the $\sqrt{3} \times \sqrt{3}$-Ag surface mainly give rise to the observed abrupt resistance drop.

Thus the observed differences in resistance changes depending on the substrate-surface structures are understood with aid of data on the microscopic atomic and electronic structures.

5. Field Effect on the Surface Conductance

Field effect experiments played an important role at the early stages of studies on surface electronic states of semiconductors about 50 years ago[23]. Surface charges induced by an electric field applied normal to the surface are captured in surface states and immobile, resulting in screening of the external field. A metallic surface such as the Si(111)-7 $\times$ 7 is expected to screen the field more effectively than a semiconducting surface such as the Si(111)-$\sqrt{3} \times \sqrt{3}$-Ag. Figure 2(c) is an illustration of our sample holder for the field effect experiment. After preparing surface superlattice structures on a Si(111) with RHEED observations,

a Ta rod is slid to face to the silicon surface with $0.2 \sim 0.3$ mm spacing. High voltage up to ± 2 kV is applied between them. The resistance change induced by the field application is measured as changes in voltage drops between the pairs of the Ta-wire contacts (on front and back sides) with small current flowing.

Preliminary results show that the field effect is actually surface-structure sensitive. For the 7×7 surface, the conductance always slightly increased with application both of negative and positive high voltages. For the $\sqrt{3} \times \sqrt{3}$-Ag surface, on the other hand, the conductance increased with positive voltage applied, while it decreased with the reversed polarity of the field. These results can not be understood simply by band-bending picture at surfaces. Defect states and surface-state conductivity must be involved for complete understanding. Further experiments with an improved sample holder are now in progress.

Acknowledgment

The present study was supported in part by a Grant-in-Aid from the Ministry of Education, Science and Culture of Japan.

References

[1] D. M. Eigler and E. K. Schweizer, Nature **344**, 524 (1990); J. A. Stroscio and D. M. Eigler, Science **254**, 1319 (1991).

[2] M. F. Crommie, C. P. Lutz and D. M. Eigler, Science **262**, 218 (1993).

[3] Y. Horikoshi, M. Kawashima, and H. Yamaguchi, Japan. J. Appl. Phys. **25**, L868 (1986).

[4] M. Copel, M. C. Renter, E. Kaxiras and R. M. Tromp, Phys. Rev. Lett. **63**, 632 (1989); S. Iwanari and K. Takayanagi, Japan. J. Appl. Phys. **30**, L1978 (1991).

[5] For a review, M. Sundaram, S. A. Chalmers, P. F. Hoptins, and A. C. Gossard, Science **254**, 1326 (1991).

[6] R. T. Tung, Phys. Rev. Lett. **52**, 461 (1984); Phys. Rev.**B45**, 13509 (1992); G. LeLay, K. Hricovini, and J. E. Bonnet, Appl. Surf. Sci. **41/42**, 25 (1989).

[7] D. R. Heslinga, H. H. Weitering, D. P. van der Werf, T. M. Klapwijk, and T. Hibma, Phys. Rev. Lett. **64**, 1589 (1990); T. Hibma, H. H. Weitering, D. R. Heslinga, and T. M. Klapwijk, Appl. Surf. Sci. **48/49**, 209 (1991).

[8] H. H. Weitering, J. P. Sullivan, R. J. Carolissen, W. R. Graham, and R. T. Tung, Appl. Surf. Sci. **70/71**, 422 (1993).

[9] S. Hasegawa and S. Ino, Phys. Rev. Lett. **68**, 1192 (1992); Surf. Sci. **283**, 438 (1993); Thin Solid Films **228**, 113 (1993); Int. J. Mod. Phys. B **7**, 3817 (1993).

[10] K. Takayanagi, Y. Tanishiro, M. Takahashi, and S. Takahashi, J. Vac. Sci. Technol. **A3** 1502 (1985); Surf. Sci. **164** 367 (1985).
[11] J. E. Demuth, B. N. J. Persson, and A. J. Schell-Sorokin, Phys. Rev. Lett. **51** 2214 (1983).
[12] R. J. Hamers, R. M. Tromp, and J. E. Demuth, Phys. Rev. Lett. **56** 1972 (1986).
[13] F. J. Himpsel, G. Hollinger, and R. A. Pollack, Phys. Rev. **B28** 7014 (1983).
[14] T. Takahashi, S. Nakatani, N. Okamoto, T. Ishikawa, and S. Kikuta, Jpn. J. Appl. Phys. **27** L753 (1988); Surf. Sci. **242** 54 (1991); Technical Report of The Institute for Solid State Physics (University of Tokyo) Ser. A, No. 2587 (1992).
[15] S. Kono, K. Higashiyama, T. Kinoshita, T. Miyahara, H. Kato, H. Ohsawa, Y. Enta, F. Maeda, and Y. Yaegashi, Phys. Rev. Lett. **58** 1555 (1987).
[16] C. S. Jiang, S. Hasegawa, and S. Ino, to be published.
[17] M. Henzler, in *Surface Physics of Materials I*, ed. J. M. Blakely (Academic Press, New York, 1975) p. 241.
[18] Y. Hasegawa, I.-W. Lyo, and Ph. Avouris, Proceedings of NATO Advanced Research Workshop on " The Ultimate Limits of Fabrication and Measurement", preprint (1994).
[19] Z. H. Zhang, S. Hasegawa, and S. Ino, to be published.
[20] A. Samsavar, T. Miller, and T. C. Chiang, Phys. Rev. **B42** 9245 (1990).
[21] St. Tosch and H. Neddermeyer, Phys. Rev. Lett. **61** 349 (1988);J. Microscopy, **152** 415 (1988); H. Neddermeyer, Critical Reviews in Solid State and Materials Sciences, **16** 309 (1990).
[22] Y. Borensztein and R. Alameh, Surf. Sci. Lett. **274** L509 (1992).
[23] J. Bardeen, Phys. Rev. **71** 717 (1947).